

Phase diagram and magnetic relaxation phenomena in Cu_2OSeO_3

F. Qian,¹ H. Wilhelm,² A. Aqeel,³ T. T. M. Palstra,³ A. J. E. Lefering,¹ E. H. Brück,¹ and C. Pappas¹

¹*Faculty of Applied Sciences, Delft University of Technology, Mekelweg 15, 2629 JB Delft, The Netherlands*

²*Diamond Light Source Ltd., Chilton, Didcot, Oxfordshire, OX11 0DE, United Kingdom*

³*Zernike Institute for Advanced Materials, University of Groningen, Nijenborgh 4, 9747 AG Groningen, The Netherlands*

(Received 7 May 2016; revised manuscript received 5 July 2016; published 15 August 2016)

We present an investigation of the magnetic-field-temperature phase diagram of Cu_2OSeO_3 based on dc magnetization and ac susceptibility measurements covering a broad frequency range of four orders of magnitude, from very low frequencies reaching 0.1 Hz up to 1 kHz. The experiments were performed in the vicinity of $T_c = 58.2$ K and around the skyrmion lattice A phase. At the borders between the different phases the characteristic relaxation times reach several milliseconds and the relaxation is nonexponential. Consequently the borders between the different phases depend on the specific criteria and frequency used and an unambiguous determination is not possible.

DOI: 10.1103/PhysRevB.94.064418

I. INTRODUCTION

In noncentrosymmetric magnetic materials Dzyaloshinskii-Moriya (DM) interactions [1,2] can stabilize two- and three-dimensional (2D and 3D) modulations with a fixed sense of rotation of the magnetization vector. These *chiral skyrmions* [3–6] in the form of axisymmetric strings have been found both in real and reciprocal space in a number of cubic helimagnets with B20 structure, such as MnSi [7,8], FeGe [9–11], $\text{Fe}_{1-x}\text{Co}_x\text{Si}$ [12–14] in the so-called A phase. This is a closed pocket of the magnetic-field (B)–temperature (T) phase diagram. The recent discovery of similar behavior in the insulator and multiferroic Cu_2OSeO_3 [15–17] has attracted attention also because in this system it is possible to manipulate skyrmions by external electric fields [18,19].

Cu_2OSeO_3 crystallizes in the noncentrosymmetric space group $P2_13$, the same as for the B20 compounds, but with two different Cu^{2+} ion sites [20,21], as shown in the inset of Fig. 1. The balance between the ferromagnetic exchange and the DM interactions leads to a long-period helical order with a pitch of ~ 70 nm [15,17]. A weak anisotropy fixes the helices along the (100) crystallographic directions below the ordering temperature T_c , which is close to 58 K. A weak external magnetic field B may overcome the anisotropy, unpin the helices from the lattice, and orient them along its direction leading to the conical phase if $B > B_{C1}$. Higher magnetic fields stabilize the A -phase pocket close to T_c and even higher magnetic fields are needed to overcome the DM interaction and the helical correlations inducing the field polarized phase, which sets in for $B > B_{C2}$ [15,17]. These features are summarized in Fig. 1, which schematically illustrates the spin arrangements of the various phases.

The phase diagram of Cu_2OSeO_3 has been investigated close to T_c by neutron scattering [15–17] and ac susceptibility for frequencies from 2.5 Hz to 1 kHz [22]. The dc magnetization and ac susceptibility measurements presented in the following complement these previous studies. Our experiments span a very broad frequency range, from 0.1 Hz to 1 kHz, which extends the previous study [22] towards the low frequencies by more than one order of magnitude. The analysis of the results as a function of the magnetic field, instead of the temperature as in the previous study, provides a

quantitative approach to the phase diagram. The dynamics at the transitions between the helical, conical, and A phases, at B_{C1} , B_{A1} , and B_{A2} , involve a broad distribution of relaxation times with characteristic times reaching several milliseconds. Additional relaxation processes have also been found at very low frequencies and around B_{C1} . The borders between the different phases are discussed and we conclude that these are not sharp but their exact location depends on the specific criteria and the frequency used. Remarkably, no relaxation is found at the high- and low-temperature boundaries of the A phase.

This paper presents and discusses the experimental results at separate sections: experimental details, magnetization, ac susceptibility at a frequency of 0.8 Hz, frequency dependence, Cole-Cole analysis, and finally the B - T phase diagram.

II. EXPERIMENTAL DETAILS

A high-quality single crystal of Cu_2OSeO_3 was grown by the chemical vapor transport method [23] and its structure was checked by x-ray diffraction. The sample with almost cubic shape was oriented with the (001) axis vertical within $\pm 5^\circ$. The magnetization M and the real and imaginary components of the ac susceptibility, χ' and χ'' respectively, were measured with a MPMS-XL Quantum Design superconducting quantum interference device magnetometer using the extraction method. A dc magnetic field B was applied along the vertical direction and parallel to the drive ac field, B_{ac} , with $0 < B_{ac} \leq 0.4$ mT, within the frequency range $0.1 \leq f \leq 1000$ Hz. Frequency scans were performed with logarithmic steps for each B and after having checked that the ac susceptibility was independent of B_{ac} , the measurements were done for $B_{ac} = 0.4$ mT. For the measurements two specific experimental protocols have been used:

(i) Field-cooled (FC) temperature scans: The sample was brought to 70 K, a magnetic field was applied, and the signal was recorded with decreasing stepwise the temperature. At each temperature the sample was brought to thermal equilibrium before measurement.

(ii) Zero-FC (ZFC) magnetic-field scans: The sample was brought to the temperature of interest under zero field (more specifically the residual field of the magnetometer which was

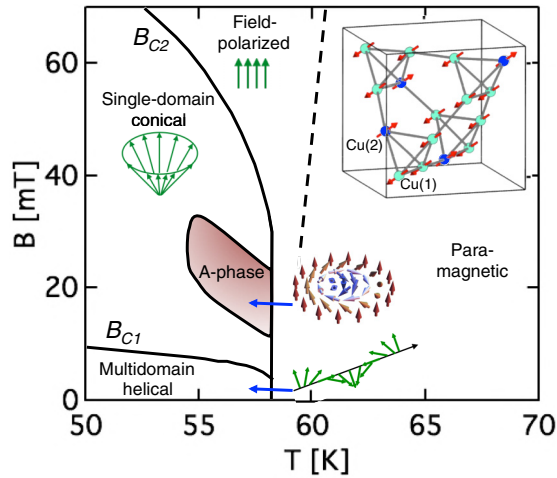


FIG. 1. Schematic representation of the phase diagram of Cu_2OSeO_3 illustrating the spin arrangements of the various phases. The inset shows the crystal structure with the two different Cu^{2+} ion sites [20].

less than 1 mT). Once thermal equilibrium was reached the measurements were performed by increasing stepwise the magnetic field.

III. MAGNETIZATION

Figure 2 displays the ZFC magnetization M and the susceptibility $\Delta M/\Delta B$, derived by numerical differentiation of the M vs B curves. The same set of data has been plotted either versus the magnetic field for selected temperatures, (a) and (c), or versus the temperature for selected magnetic fields, (b) and (d), in order to better emphasize the occurring phase transitions. The magnetization curves in panels (a) and (b) highlight the transition from the paramagnetic to the helical phase around 58 K, seen both in the strong nonlinearities of M vs B for $56 \text{ K} \lesssim T \lesssim 59 \text{ K}$ (a) and the onset of a plateau at the M vs T plots (b). The M vs B plots give only a coarse overview and the effects related with the onset of the A phase are only brought out by the $\Delta M/\Delta B$ curves, which show clear dips at $56 \text{ K} \lesssim T \lesssim 58 \text{ K}$ and $15 \text{ mT} \lesssim B \lesssim 30 \text{ mT}$. Thus the relevant features are seen on $\Delta M/\Delta B$ and show up with much higher accuracy on the ac susceptibility which will be discussed in the following sections.

IV. AC SUSCEPTIBILITY AT 0.8 Hz

Figure 3 shows the temperature dependence of χ' measured at $B = 0 \text{ mT}$ and at a frequency of 0.8 Hz. For $B = 0 \text{ mT}$ and all frequencies used in this work χ' was frequency independent and $\chi'' = 0$. The peak at $T_c = 58.20 \pm 0.05 \text{ K}$ marks the transition to the helical state and the closer inspection shown in the inset reveals an asymmetric cusplike shape with a shoulder at $\sim 58.6 \text{ K}$, as reported before in Cu_2OSeO_3 [22,24]. Similarly to MnSi [25] the shoulder marks the onset of the precursor phase [26], where helical correlations and fluctuations become predominant.

In the helical phase χ' varies nonmonotonically showing a minimum at $\sim 57 \text{ K}$ and a broad maximum at about

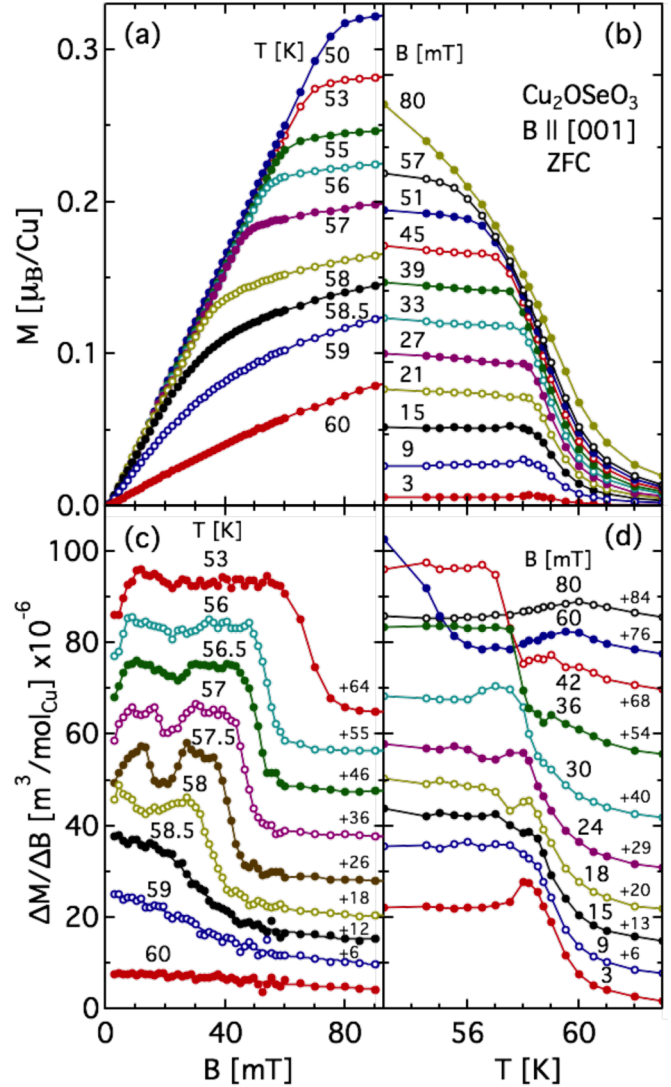


FIG. 2. ZFC magnetization of Cu_2OSeO_3 as a function of temperature and magnetic field. The same set of data has been plotted vs the magnetic field for selected temperatures (a) and vs the temperature for selected magnetic fields (b). The susceptibility $\Delta M/\Delta B$ deduced by numerical differentiation of the M vs B curves is shown as a function of the magnetic field in (c) and of temperature in (d). For the sake of clarity the curves in (c) and (d) have been shifted vertically with respect to the baseline by the values indicated.

30 K before levelling off to $\sim 23 \times 10^{-6} \text{ m}^3/\text{mol}_{\text{Cu}}$ below 10 K. This value is comparable to the one reported for a polycrystalline sample [20], where however a smoother temperature dependence with no clear peak at T_c has been found. On the other hand, the overall shape of χ' in Fig. 3 is similar to the one found for another single crystal along $\langle 111 \rangle$, where slightly lower absolute values have been reported possibly due to the different crystal orientations [27].

At low temperatures the magnetic response depends on the magnetic history of the sample. It has indeed been found that below 50 K FC and ZFC measurements give different results [20,24]. For this reason we distinguished between FC or ZFC following the specific procedures described above. The results did not show any influence of the magnetic history on

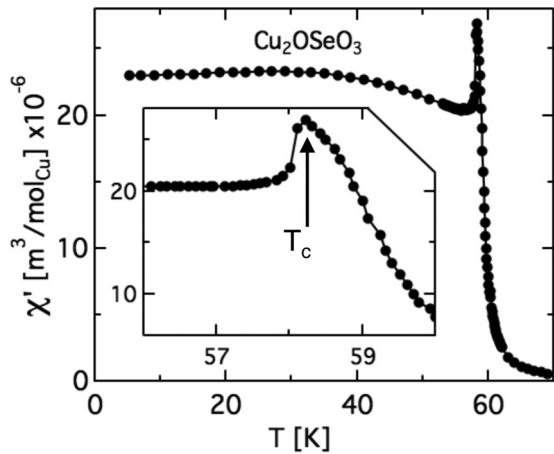


FIG. 3. Temperature dependence of χ' of Cu_2OSeO_3 for $B = 0$ mT and $f = 0.8$ Hz. The inset shows a closeup around the peak, which marks the onset of the helical order and reveals an asymmetric shape with a shoulder above $T_c = 58.20 \pm 0.05$ K.

the susceptibility. Despite that, for the sake of clarity, we will specify in the following the protocol used for each set of data.

Figure 4 shows the FC susceptibility, χ' , (a) and (b), and χ'' , (c) and (d), in the vicinity of T_c for selected values of B and reveals the strong influence of the magnetic field: the peak of χ' , which has been associated with T_c at $B = 0$, shifts to lower temperatures whereas the high-temperature shoulder becomes more noticeable. At 12 mT $\lesssim B \lesssim 23$ mT the shape of χ' changes dramatically: it shows two maxima separated by a minimum characteristic for the A phase. By further increasing the magnetic field only one cusp remains and the shape becomes again similar to that of low fields. Much higher magnetic fields smoothen the cusp and χ' becomes almost temperature independent below ~ 58 K.

The magnetic field has a dramatic influence also on χ'' . The weakest magnetic field (3 mT in our case) induces already a peak in χ'' slightly below T_c , which becomes more pronounced at 5 mT and transforms into a broad maximum upon further increasing the field. Between 14 and 17 mT the maximum becomes a strong and well defined cusp. By further increasing B , χ'' vanishes for 21 mT $< B < 23$ mT but re-appears for $B > 23$ mT before fading away at higher fields approaching B_{C2} .

A complementary view of the effect of temperature and magnetic field is given by Fig. 5, where the ZFC susceptibility is plotted versus the magnetic field for selected temperatures. Well above T_c , at 60.5 K, χ' is almost field independent and χ'' is practically zero. Lowering the temperature leads to a strong increase of the low field χ' . Furthermore, at T_c a nonmonotonic behavior develops with a minimum at $B \sim 14$ mT, which is characteristic for the A phase. The minimum is most pronounced for 58 K $\gtrsim T \gtrsim 57$ K and persists down to 55 K.

As already mentioned χ'' is zero for $T \geq T_c$ and for all frequencies used in this study. A peak first appears at 58 K centered at $B = 4$ mT and remains significant upon decreasing the temperature. At 57.8 K two additional maxima appear at the borders of the A phase, which evolve to well defined peaks at 57 K and fade out at lower temperatures.

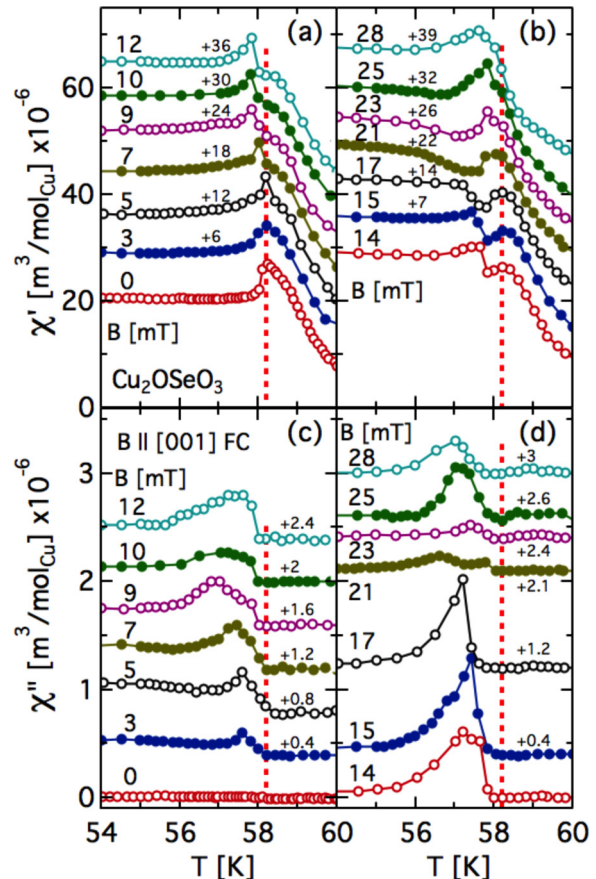


FIG. 4. Temperature dependence of FC χ' (a),(b) and χ'' (c),(d) for different magnetic fields B and for $f = 0.8$ Hz. The vertical dashed lines indicate T_c for $B = 0$. For the sake of clarity the curves have been shifted vertically with respect to the base line by the numbers given next to each of them.

Both χ' and χ'' bear the signature of the series of field-induced transitions characteristic of Cu_2OSeO_3 [17,22,28] and helimagnets of B20 types such as MnSi [7,29] or FeGe [10,11]. Below T_c the application of a magnetic field induces an initial increase of χ' related to the transition from the helical to the conical phases at the lower critical field B_{C1} . By further increasing the magnetic field at sufficiently low temperatures, for Cu_2OSeO_3 at $T < 55$ K, χ' remains constant until the upper critical field B_{C2} , where it decreases rapidly indicating the transition to the field polarized state. Besides this generic scheme, very close to T_c additional features appear both in χ' and χ'' in relation with the boundaries of the A phase.

The extraction of an exact phase diagram however, with precise values for the critical fields is not an easy task as the result very much depends on the specific criteria used. This is illustrated by Fig. 6, that displays the magnetic-field dependence of the ZFC χ' , its first derivative $d\chi'/dB$, and the corresponding χ'' at $T = 57.3$ K, a characteristic temperature where all features are present. One may indeed choose either the inflection points of χ' or the maxima of χ'' to define the phase boundaries. Both choices are valid and would lead to magnetic fields with similar temperature dependence. We chose the peaks of χ'' at $f = 0.8$ Hz to define B_{C1} and the boundaries of the A phase, B_{A1} and B_{A2} respectively. On the

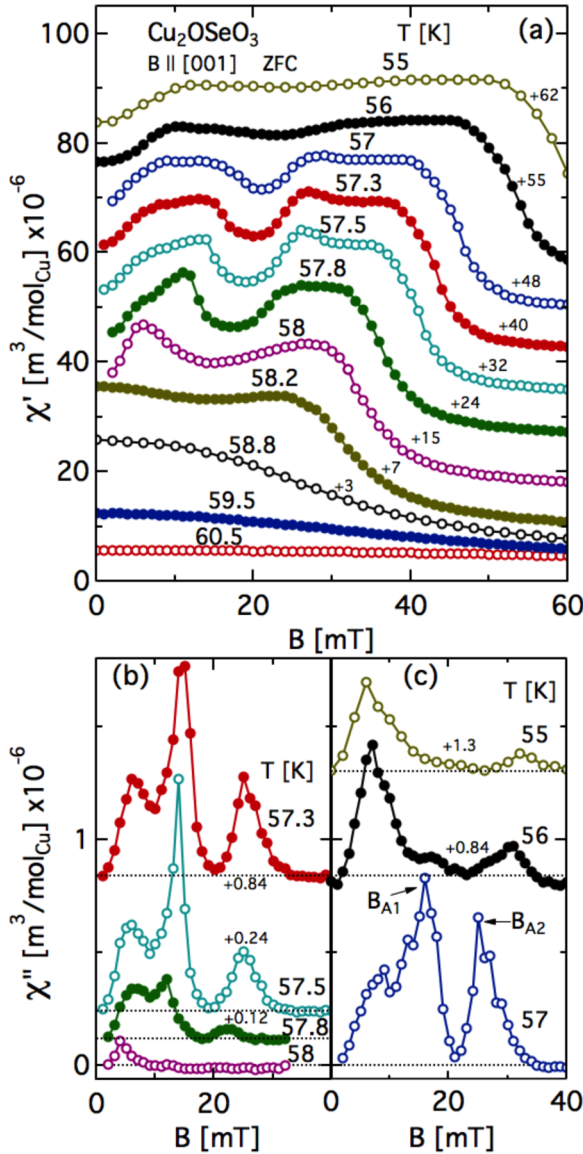


FIG. 5. Magnetic-field dependence of ZFC χ' (a) and χ'' (b),(c) of Cu_2OSeO_3 for some selected temperatures and for $f = 0.8$ Hz. For the sake of clarity some curves have been vertically shifted with respect to the base line by the values indicated next to each of them.

other hand χ'' is zero at high fields and for this reason B_{C2} was defined from the inflection point of χ' . The lower and upper boundaries of this transition can be estimated from the extrema of the second derivative $d^2\chi'/dB^2$ (thus the inflection points of the first derivative $d\chi'/dB$), which are given by the red dotted lines in Fig. 6(b) and will be discussed at the phase diagram section below.

A clear overview of the phase diagram and the transitions between the helical, conical, A, and field polarized phases respectively is only provided by the analysis as a function of the magnetic field presented above. If only the temperature dependence of the susceptibility is considered, as it was the case in the previous study [22], the different contributions merge into broad features as illustrated by Fig. 4(c), in particular between 9 and 12 mT, and thus no clear indications for the phase boundaries can be obtained.

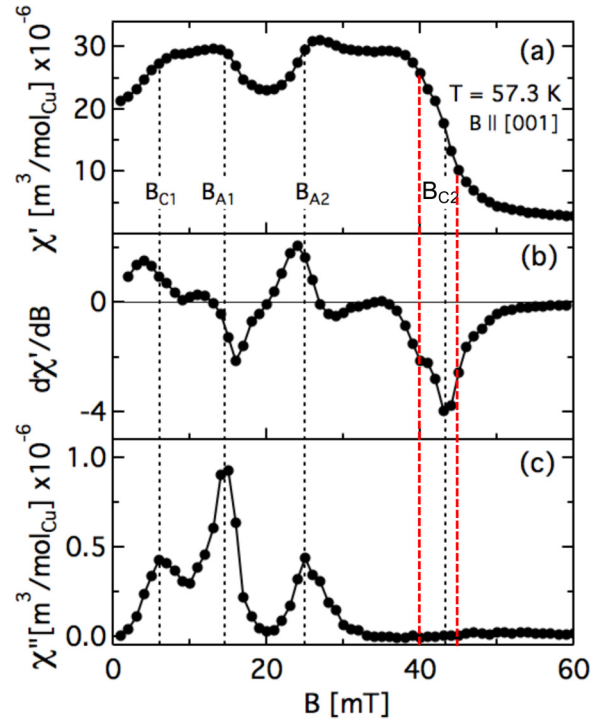


FIG. 6. Magnetic-field dependence of ZFC χ' , its derivative $d\chi'/dB$, and the corresponding χ'' of Cu_2OSeO_3 at $T = 57.3$ K for $B \parallel [001]$ and $f = 0.8$ Hz. The maxima of χ'' define the lower critical field $B_{C1} = 6$ mT as well as the lower and upper boundaries of the A phase, $B_{A1} = 14.5$ mT and $B_{A2} = 25$ mT, respectively. The upper critical field ($B_{C2} = 43$ mT) was determined from the inflection points of χ' and the extrema of $d\chi'/dB$. The red dotted lines correspond to the inflection points of $d\chi'/dB$ at the two sides of B_{C2} and thus to the lower and upper boundaries of this transition. The unit of $d\chi'/dB$ is $\text{m}^3/(\text{mol}_{\text{Cu}} \text{mT}) \times 10^{-6}$.

V. FREQUENCY DEPENDENCE OF χ' AND χ''

The previous section discussed results at $f = 0.8$ Hz. However, the susceptibility depends on the frequency of the ac drive field as highlighted by Fig. 7, where ZFC χ' and χ'' are displayed versus the magnetic field for some selected frequencies and $T = 57.3$ K. The minimum in χ' , which is characteristic for the A phase, is best defined at low frequencies. With increasing frequency, the minimum broadens, accompanied by a decreasing amplitude of the humplike edges at both sides. The most dramatic changes are found for χ'' , which at 0.35 Hz displays the three well-defined maxima related to the phase boundaries B_{C1} , B_{A1} , and B_{A2} . The amplitude of these maxima changes with frequency but their position remains roughly the same.

A more detailed overview of the effect of frequency is given in Fig. 8, where χ' and χ'' are displayed as a function of frequency for selected magnetic fields around $B_{C1} = 6$ mT, (a) and (d), $B_{A1} = 14.5$ mT, (b) and (e), and $B_{A2} = 25$ mT, (c) and (f), at $T = 57.3$ K. As already mentioned and illustrated by Fig. 7, χ' does not depend on the frequency for $B = 0$ and $\chi'' = 0$. However, even weak magnetic fields induce noticeable effects shown in both Figs. 7 and 8. The broad bell-shaped frequency dependence of χ'' seen in Figs. 8(d)–8(f) reflects a distribution of relaxation frequencies centered at the

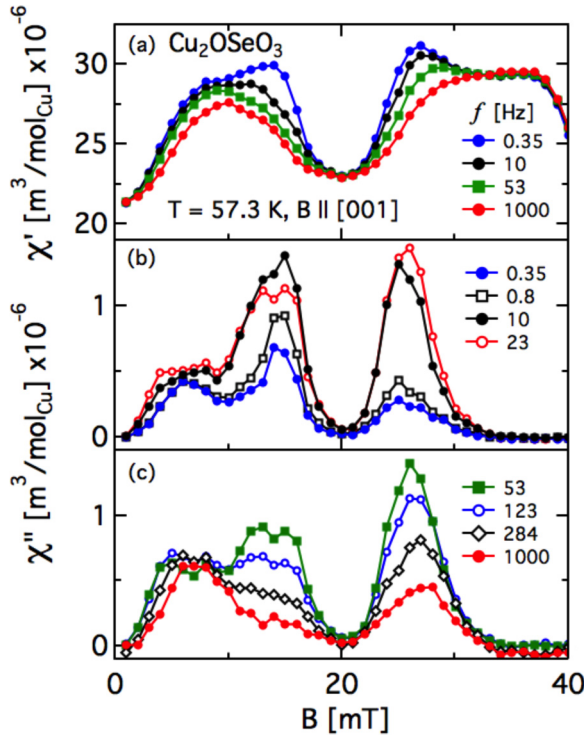


FIG. 7. Magnetic-field dependence of ZFC χ' (a) and χ'' (b),(c) of Cu_2OSeO_3 at $T = 57.3$ K and for the frequencies indicated.

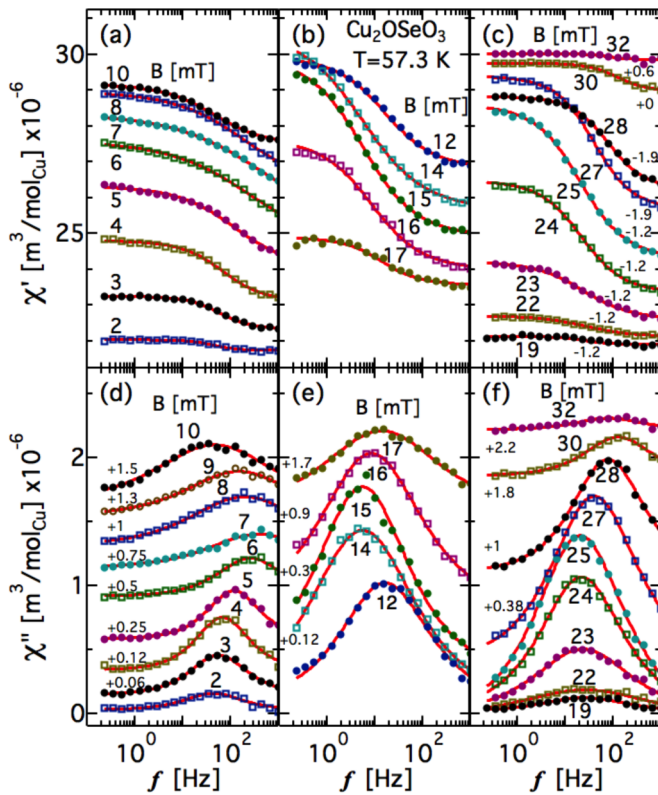


FIG. 8. Frequency dependence of ZFC χ' and χ'' of Cu_2OSeO_3 at $T = 57.3$ K for magnetic fields around B_{C1} (a),(d), B_{A1} (b),(e), and B_{A2} (c),(f) respectively. The lines represent fits of Eqs. (2) and (3). For the sake of clarity some data sets in panels (c)–(f) have been vertically shifted with respect to the baseline as indicated.

characteristic frequency f_0 , which varies nonmonotonically around B_{C1} , B_{A1} , and B_{A2} . Similar behavior has already been reported for Cu_2OSeO_3 [22] and the quantitative analysis is based on the modified Cole-Cole formalism [30,31]:

$$\chi(\omega) = \chi(\infty) + \frac{\chi(0) - \chi(\infty)}{1 + (i\omega\tau_0)^{1-\alpha}} \quad (1)$$

with $\chi(0)$ and $\chi(\infty)$ the isothermal and adiabatic susceptibilities, $\omega = 2\pi f$ the angular frequency, $\tau_0 = 1/(2\pi f_0)$ the characteristic relaxation time, and α a parameter that accounts for the width of the relaxation frequencies distribution, $\alpha = 1$ for an infinitely broad distribution, and $\alpha = 0$ for a single relaxation process. Thus $\alpha = 0$ corresponds to a simple exponential and $\alpha > 0$ to a stretched exponential relaxation, which can be attributed to a distribution of energy barriers in a phase-space landscape [32]. Equation (1) can be decomposed in the in- and out-of-phase components [31,33]:

$$\chi'(\omega) = \chi(\infty) + \frac{A_0 [1 + (\omega\tau_0)^{1-\alpha} \sin(\pi\alpha/2)]}{1 + 2(\omega\tau_0)^{1-\alpha} \sin(\pi\alpha/2) + (\omega\tau_0)^{2(1-\alpha)}}, \quad (2)$$

$$\chi''(\omega) = \frac{A_0 \cos(\pi\alpha/2) (\omega\tau_0)^{1-\alpha}}{1 + 2(\omega\tau_0)^{1-\alpha} \sin(\pi\alpha/2) + (\omega\tau_0)^{2(1-\alpha)}} \quad (3)$$

with $A_0 = \chi(0) - \chi(\infty)$. The fit of these equations to the data leads to the solid lines in Fig. 8 and the parameters, $f_0 = 1/(2\pi\tau_0)$, α and A_0 are plotted as a function of the magnetic field in Fig. 9.

The characteristic frequency f_0 shown in Fig. 9(a) is derived from the maxima of χ'' and varies nonmonotonically with B . First a maximum develops slightly above B_{C1} , indicating the acceleration of the dynamics at the border between the helical and conical phases. Then clear minima, reflecting a slowing down of the relaxation, mark the limits of the A phase B_{A1} and B_{A2} respectively.

The parameter α given in Fig. 9(b) shows no clear trends, but remains nonzero over the whole magnetic-field range, as previously found [22]. This implies a stretched exponential relaxation similar to spin glasses [31,33] and is in agreement with the glassiness found by electron microscopy for Cu_2OSeO_3 [34] and other systems with similarly long helices [35].

The prefactor $A_0 = \chi(0) - \chi(\infty)$ given in Fig. 9(c) shows clear maxima at B_{C1} , B_{A1} , and B_{A2} . Consequently at these characteristic fields the difference between $\chi(0)$ and $\chi(\infty)$ is the strongest and the magnetic relaxation phenomena are most prominent.

For $B < 10$ mT, which includes B_{C1} , the fit of χ' and χ'' does not lead to the same values for α and A_0 , indicating the existence of an additional process. Indeed in this magnetic-field range an almost frequency-independent component, designated by χ_0'' and shown in Fig. 9(d), exists that is most visible on χ'' and is at the origin of the different A_0 values derived from χ' and χ'' . As it will be discussed below it is also seen on the Cole-Cole plots.

The magnetic-field dependence of f_0 , α , A_0 , and χ_0'' derived from χ'' is given in Fig. 10 for some selected temperatures. The figure shows the same trends as Fig. 9. The relaxation involves indeed macroscopic characteristic times,

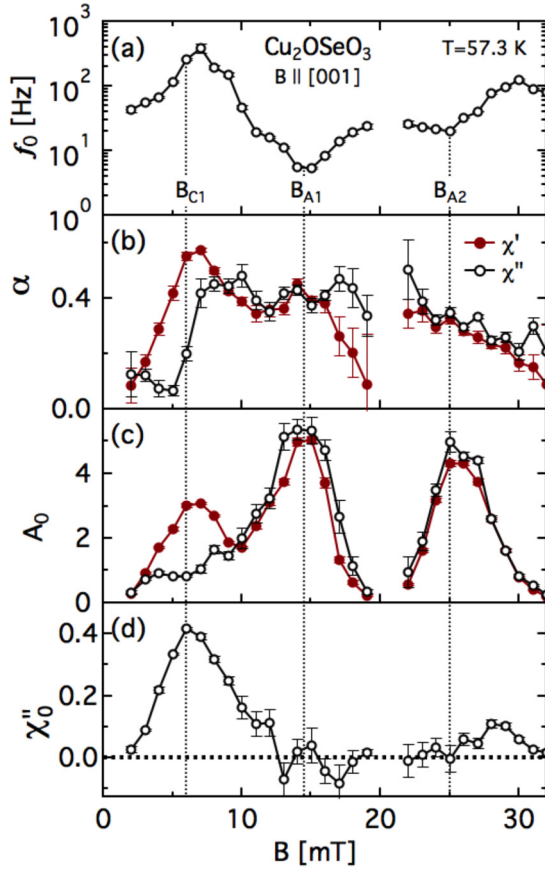


FIG. 9. Magnetic-field dependence of (a) the characteristic frequency f_0 , (b) the relaxation times distribution parameter α , and (c) $A_0 = \chi(0) - \chi(\infty)$ as defined by Eq. (2). The open and closed symbols correspond to the parameters extracted from χ'' and χ' respectively. The phase boundaries B_{C1} , B_{A1} , and B_{A2} are indicated by the vertical dashed lines. No fits are possible in the center of the A phase, which explains the absence of points. Panel (d) displays a frequency independent component χ''_0 , which is required to fit χ'' around B_{C1} and accounts for the different A_0 derived from χ' and χ'' respectively. The units of A_0 and χ''_0 are $\text{m}^3/\text{mol}_{\text{Cu}} \times 10^{-6}$.

which reflect rearrangements over large magnetic volumes. We note that all maxima and minima of f_0 and A_0 are correlated with the phase boundaries B_{C1} , B_{A1} , and B_{A2} .

Figure 10(a) shows that f_0 is almost temperature independent at B_{C1} but varies strongly with temperature at B_{A1} and B_{A2} . At these magnetic fields a simple Arrhenius law $f_0 = A \exp(-E/k_B T)$ implies a linear dependence of $\ln(f_0)$ on $1/T$. As seen in Fig. 10(e) this is in general not the case. Furthermore, an Arrhenius fit to the data leads to unphysically large energy barriers of the order of 10^4 K. Thus the temperature dependence of the relaxation cannot be accounted for by a simple thermal activation picture.

VI. COLE-COLE ANALYSIS

The Cole-Cole formalism interrelates χ' and χ'' and from Eqs. (2) and (3) one deduces

$$\chi''(\omega) = -B_0 + [B_0^2 + A_0[\chi'(\omega) - \chi(\infty)] - [\chi'(\omega) - \chi(\infty)]^2]^{1/2} \quad (4)$$

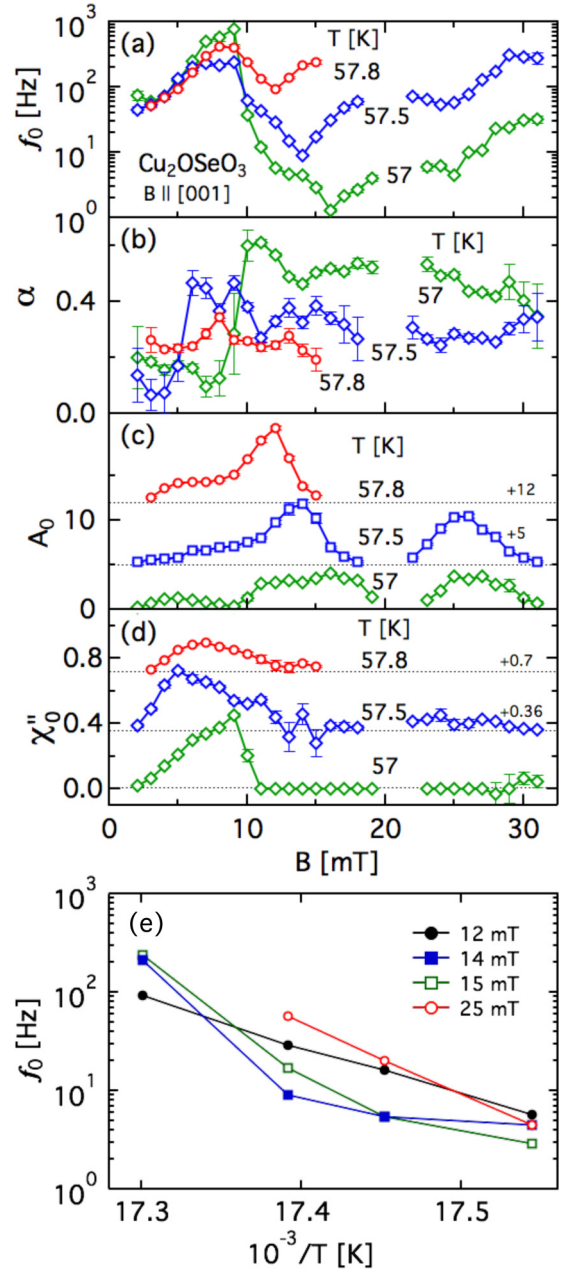


FIG. 10. Magnetic-field dependence of (a) the characteristic frequency f_0 , (b) the relaxation times distribution parameter α , (c) the amplitude $A_0 = \chi(0) - \chi(\infty)$, and (d) the constant term χ''_0 for the temperatures indicated, obtained from the fits of Eq. (3) to χ'' of Cu_2OSeO_3 . For the sake of clarity some A_0 and χ''_0 curves have been shifted with respect to the baseline as indicated. No fits are possible in the center of the A phase and above 15 mT for 57.8 K, which explains the absence of points. The units of A_0 and χ''_0 are $\text{m}^3/\text{mol}_{\text{Cu}} \times 10^{-6}$. Panel (e) shows the temperature dependence of f_0 from panel (a) for various magnetic fields.

with $B_0 = A_0 \tan(\pi\alpha/2)/2$. This relation has three free parameters, $\chi(\infty)$, A_0 , and α , and corresponds to the equation of a circular arc centered at the maximum of χ'' , where $\omega\tau_0 = 1$. Resulting Cole-Cole plots are shown in Fig. 11, where the ZFC data of Fig. 8 have been replotted for selected magnetic fields. The Cole-Cole plots for one relaxation process are

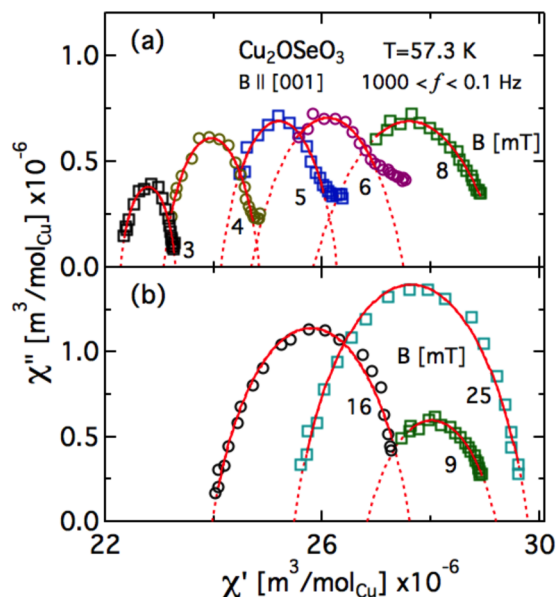


FIG. 11. Cole-Cole plots of Cu_2OSeO_3 for various magnetic fields at $T = 57.3$ K. The dashed lines represent the fits of Eq. (4) to the data.

symmetric and centered at $\chi' = [\chi(0) + \chi(\infty)]/2$, where χ'' is maximum. As the parameter α is proportional to the ratio of

the bottom width to the height of the curves, the plots directly evidence the existence of a distribution of relaxation times.

The data fall on a circular arc as expected by Eq. (4) and are well described for all magnetic fields except for $4 \text{ mT} \lesssim B \lesssim 8 \text{ mT}$, where significant deviations at the highest values of χ' , which correspond to the lowest frequencies, are observed. This is indeed the magnetic-field range, where Eqs. (2) and (3) do not give consistent results for both χ' and χ'' as witnessed by the different values of A_0 and α shown in Fig. 9 and the frequency independent term χ''_0 that must be considered to properly account for χ'' . These deviations reveal the existence of additional relaxation mechanisms, the origin of which is unknown. In analogy to ferromagnets we speculate that they may be due to domain-wall motion and coexist with the main dynamic process associated with the helical to conical phase transition. Indeed these deviations disappear above B_{C1} where the system becomes monodomain under the influence of the strong external magnetic field.

VII. PHASE DIAGRAM

The magnetic-field, temperature, and frequency dependence of χ' and χ'' are summarized by the contour plots of Fig. 12 for $f = 0.8$ Hz, 23 Hz, and 1 kHz. The frequency has a weak effect on χ' in contrast to χ'' . The contour plots also illustrate the differences in the frequency dependence around B_{C1} on one side and around B_{A1} or B_{A2} on the other side, addressed at the previous sections; e.g., see Fig. 7.

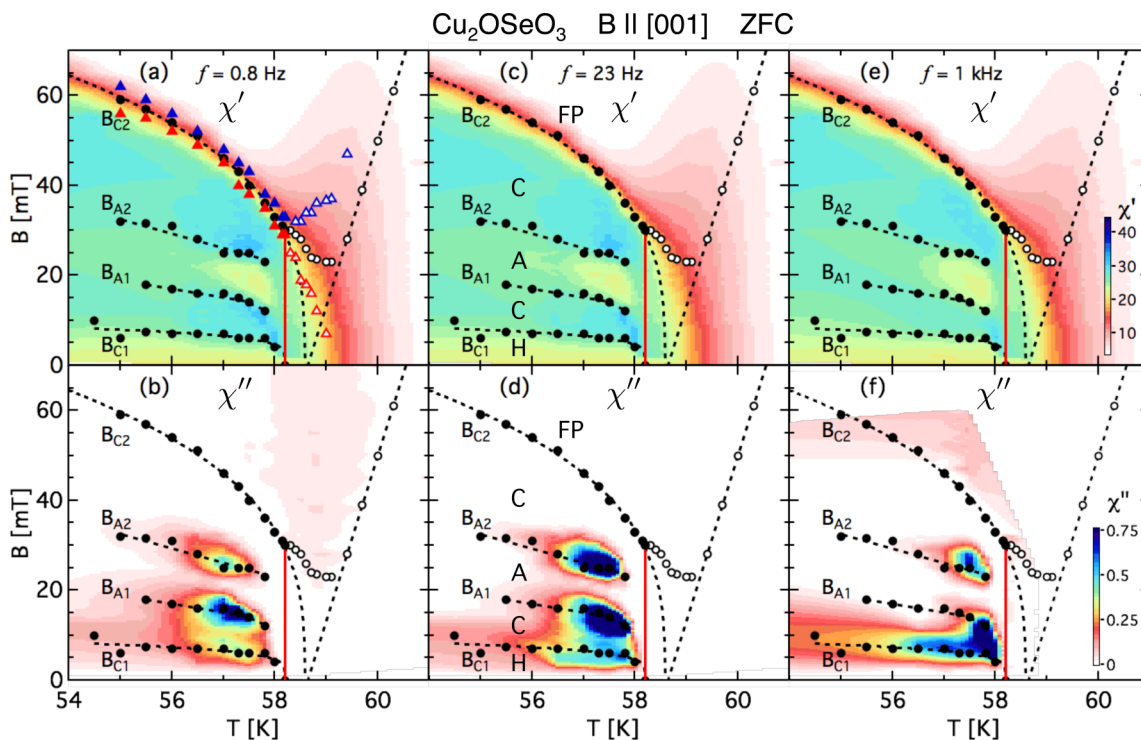


FIG. 12. Contour plots of ZFC χ' and χ'' of Cu_2OSeO_3 measured at the frequencies $f = 0.8$ Hz (a),(b), 23 Hz (c),(d), and 1 kHz (e),(f) displayed vs temperature and magnetic field. The values given at the color codes correspond to $\text{m}^3/\text{mol}_{\text{Cu}} \times 10^{-6}$. The vertical red lines indicate T_c at $B = 0$. The characteristic magnetic fields B_{C1} , B_{A1} , B_{A2} , and B_{C2} determined at 0.8 Hz are also indicated. The lower and upper boundaries of the transition at B_{C2} are illustrated in panel (a) by the red and blue triangles determined from the inflection points of $d\chi'/dB$. Above T_c the extrema of the first and second derivatives of χ' are illustrated with open symbols to distinguish from B_{C2} below T_c . In panels (c) and (d) we identify the following phases: H for helical, C for conical, A for the A phase, and FP for the field polarized one.

Consequently, the strongest χ'' in Fig. 12 is for $f = 23$ Hz at B_{A1} or B_{A2} , and for $f = 1$ kHz at B_{C1} . At this highest frequency the phase boundaries seen in χ'' almost obliterate.

Very weak signals in χ'' appear for $B > B_{C2}$ in panels (b) and (f). The origin of the χ'' at $f = 0.8$ Hz is unclear and we plan to investigate this feature more in detail in the future. We note that similar features have been found also at very low frequencies in MnSi and the soliton lattice system $\text{Cr}_{1/3}\text{NbS}_2$ [36]. On the other hand, the signal at 1 kHz may be associated with the spin dynamics in the field-polarized phase. In this phase the magnetic field is strong enough to overcome the DM interaction and the behavior crosses over to ferromagnetism with clear susceptibility maxima developing above T_c . These shift to higher temperatures with increasing magnetic field, as shown in Fig. 2(d) and in the χ' contour plots of Figs. 12(a), 12(c), and 12(e).

Below T_c the temperature dependence of B_{C2} is described by the power law $B_{C2} \propto (T - T_0)^{0.318 \pm 0.03}$ with $T_0 = 58.6 \pm 0.15$ K, i.e., $\sim T_c + 0.4$ K. The extrapolation of this power law to low fields is given by the black dashed lines in Fig. 12 and is in good agreement with the contour plots of χ' . The lower and upper magnetic-field limits deduced from the inflection points of $d\chi'/dB$, as illustrated by the red dotted lines in Fig. 6, are also given by the red and blue triangles in Fig. 12(a). These are very close to B_{C2} deduced from the first derivative of χ' [black dots in Fig. 12(a)] and follow the same power law. Thus the result is not affected by the specific criterion used and the sharpness of the transition.

Above T_c , the steep change of χ' at B_{C2} , reflected by the sharp minimum of the first derivative $d\chi'/dB$ in Fig. 6, broadens with increasing temperature. In order to distinguish it from B_{C2} below T_c , the inflection point of χ' above T_c is illustrated with open circles. It goes through a minimum at ~ 59 K and for higher temperatures increases linearly with temperature, extrapolating to $T_0 = 58.6$ K at zero field. This linear temperature dependence of the inflection points of χ' at high fields can also be derived from a magnetization Brillouin function. In this case, similarly to the Curie-Weiss law for the susceptibility, T_0 corresponds to the mean-field average of the interactions and is equivalent to a Curie-Weiss temperature.

For $B < B_{C2}$ the plots of Fig. 12 reveal the areas associated with the helical, conical, and A phases respectively. On the χ' plots, Figs. 12(a), 12(c), and 12(e), the yellowish area below the B_{C1} line corresponds to the helical phase, whereas the light blue areas between B_{C1} and B_{A1} and between B_{A2} and B_{C2} correspond to the conical phase. Between B_{A1} and B_{A2} , a yellowish area with almost a triangular shape at low frequencies stands for the center of the A phase. The high-temperature limits of the A phase are better defined than the low-temperature ones, where below ~ 57 K a rather gradual crossover from the A phase to the conical is observed.

Remarkably neither the high-temperature nor the low-temperature limits of the A phase are seen on χ'' , Figs. 12(b), 12(d), and 12(f), in contrast to the clear delimitation of the low and upper magnetic-field limits B_{A1} and B_{A2} respectively. We note that this result does not depend on the way the measurements were performed: temperature scans at constant magnetic fields (FC) and magnetic-field scans at constant temperatures (ZFC) give exactly the same results within the experimental accuracy. Thus the temperature induced transitions into and out of the A phase are not equivalent to the magnetic-field induced ones. In MnSi the (first-order phase transition) upper temperature limits of the A phase are clearly seen by specific heat but not in χ'' for $f = 1$ kHz [37]. This might also explain the absence of χ'' for the temperature limit of the A phase in Cu_2OSeO_3 as well.

The absence of a clear low-temperature boundary of the A phase on χ'' may be another indication for a gradual crossover to the conical phase seen by χ' . In such a case the magnetic relaxation phenomena might be spread over a broad temperature range and the resulting χ'' signal might become too weak to be detected.

VIII. CONCLUSION

The analysis of the dc magnetization and ac susceptibility of Cu_2OSeO_3 as a function of the magnetic field, instead of the temperature as in previous studies, provides a quantitative approach to the phase diagram. The investigation of the B - T phase diagram of Cu_2OSeO_3 by dc magnetization and ac susceptibility shows that the borders between the different phases (helical, conical, and A phase) are not sharp but their exact position depends on the specific technique and criteria used. The frequency dependence of χ'' , between the helical and conical phases at B_{C1} and between the conical and A phases at B_{A1} and B_{A2} , is governed by almost macroscopic relaxation times, which reach some milliseconds and may be attributed to rearrangements over large magnetic volumes. An additional relaxation process has also been found, which appears only at very low frequencies and around B_{C1} . The strongly nonexponential relaxation bears similarities with spin glasses and is in line with the glassy behavior reported by electron microscopy in Cu_2OSeO_3 and other systems with similarly long helices. The dynamical phenomena discussed at the previous sections could be at the origin of the different phase boundaries reported in the literature not only for Cu_2OSeO_3 but also for other systems of the same family including the reference chiral magnet MnSi.

ACKNOWLEDGMENTS

The authors would like to thank M. Mostovoy and G. R. Blake for fruitful discussions. F.Q. acknowledges financial support from China Scholarship Council (CSC).

[1] I. Dzyaloshinsky, *J. Phys. Chem. Solids* **4**, 241 (1958).

[2] T. Moriya, *Phys. Rev.* **120**, 91 (1960).

[3] A. N. Bogdanov and D. A. Yablonskii, *Zh. Eksp. Teor. Fiz.* **95**, 178 (1989) [*Sov. Phys. JETP* **68**, 101 (1989)].

[4] A. Bogdanov and A. Hubert, *J. Magn. Magn. Mater.* **138**, 255 (1994).

[5] U. K. Rößler, A. A. Leonov, and A. N. Bogdanov, *J. Phys.: Conf. Ser.* **303**, 012105 (2011).

- [6] N. Nagaosa and Y. Tokura, *Nat. Nanotechnol.* **8**, 899 (2013).
- [7] S. Mühlbauer, B. Binz, F. Jonietz, C. Pfleiderer, A. Rosch, A. Neubauer, R. Georgii, and P. Böni, *Science* **323**, 915 (2009).
- [8] A. Tonomura, X. Yu, K. Yanagisawa, T. Matsuda, Y. Onose, N. Kanazawa, H. S. Park, and Y. Tokura, *Nano Lett.* **12**, 1673 (2012).
- [9] X. Z. Yu, N. Kanazawa, Y. Onose, K. Kimoto, W. Z. Zhang, S. Ishiwata, Y. Matsui, and Y. Tokura, *Nat. Mater.* **10**, 106 (2010).
- [10] H. Wilhelm, M. Baenitz, M. Schmidt, U. K. Rößler, A. A. Leonov, and A. N. Bogdanov, *Phys. Rev. Lett.* **107**, 127203 (2011).
- [11] E. Moskvin, S. Grigoriev, V. Dyadkin, H. Eckerlebe, M. Baenitz, M. Schmidt, and H. Wilhelm, *Phys. Rev. Lett.* **110**, 077207 (2013).
- [12] X. Z. Yu, Y. Onose, N. Kanazawa, J. H. Park, J. H. Han, Y. Matsui, N. Nagaosa, and Y. Tokura, *Nature (London)* **465**, 901 (2010).
- [13] W. Münzer, A. Neubauer, T. Adams, S. Mühlbauer, C. Franz, F. Jonietz, R. Georgii, P. Böni, B. Pedersen, M. Schmidt, A. Rosch, and C. Pfleiderer, *Phys. Rev. B* **81**, 041203(R) (2010).
- [14] H. S. Park, X. Yu, S. Aizawa, T. Tanigaki, T. Akashi, Y. Takahashi, T. Matsuda, N. Kanazawa, Y. Onose, D. Shindo, A. Tonomura, and Y. Tokura, *Nat. Nanotechnol.* **9**, 337 (2014).
- [15] S. Seki, X. Z. Yu, S. Ishiwata, and Y. Tokura, *Science* **336**, 198 (2012).
- [16] S. Seki, J. H. Kim, D. S. Inosov, R. Georgii, B. Keimer, S. Ishiwata, and Y. Tokura, *Phys. Rev. B* **85**, 220406(R) (2012).
- [17] T. Adams, A. Chacon, M. Wagner, A. Bauer, G. Brandl, B. Pedersen, H. Berger, P. Lemmens, and C. Pfleiderer, *Phys. Rev. Lett.* **108**, 237204 (2012).
- [18] J. S. White, I. Levatić, A. A. Omrani, N. Egetenmeyer, K. Prša, I. Živković, J. L. Gavilano, J. Kohlbrecher, M. Bartkowiak, H. Berger, and H. M. Rønnow, *J. Phys.: Condens. Matter* **24**, 432201 (2012).
- [19] J. S. White, K. Prša, P. Huang, A. A. Omrani, I. Živković, M. Bartkowiak, H. Berger, A. Magrez, J. L. Gavilano, G. Nagy, J. Zang, and H. M. Rønnow, *Phys. Rev. Lett.* **113**, 107203 (2014).
- [20] J.-W. G. Bos, C. V. Colin, and T. T. M. Palstra, *Phys. Rev. B* **78**, 094416 (2008).
- [21] M. Belesi, I. Rousochatzakis, H. C. Wu, H. Berger, I. V. Shvets, F. Mila, and J. P. Ansermet, *Phys. Rev. B* **82**, 094422 (2010).
- [22] I. Levatić, V. Šurija, H. Berger, and I. Živković, *Phys. Rev. B* **90**, 224412 (2014).
- [23] K. H. Miller, X. S. Xu, H. Berger, E. S. Knowles, D. J. Arenas, M. W. Meisel, and D. B. Tanner, *Phys. Rev. B* **82**, 144107 (2010).
- [24] I. Živković, D. Pajić, T. Ivek, and H. Berger, *Phys. Rev. B* **85**, 224402 (2012).
- [25] S. M. Stishov, A. E. Petrova, S. Khasanov, G. K. Panova, A. A. Shikov, J. C. Lashley, D. Wu, and T. A. Lograsso, *Phys. Rev. B* **76**, 052405 (2007).
- [26] S. M. Stishov and A. E. Petrova, [arXiv:1606.06922](https://arxiv.org/abs/1606.06922).
- [27] I. Živković, J. S. White, H. M. Rønnow, K. Prša, and H. Berger, *Phys. Rev. B* **89**, 060401(R) (2014).
- [28] S. Seki, S. Ishiwata, and Y. Tokura, *Phys. Rev. B* **86**, 060403(R) (2012).
- [29] A. Bauer and C. Pfleiderer, *Phys. Rev. B* **85**, 214418 (2012).
- [30] K. S. Cole and R. H. Cole, *J. Chem. Phys.* **9**, 341 (1941).
- [31] D. Huser, A. J. van Duynveldt, G. J. Nieuwenhuys, and J. A. Mydosh, *J. Phys. C: Solid State Phys.* **19**, 3697 (1986).
- [32] I. A. Campbell, *Phys. Rev. B* **33**, 3587 (1986).
- [33] C. Dekker, A. F. M. Arts, H. W. de Wijn, A. J. van Duynveldt, and J. A. Mydosh, *Phys. Rev. B* **40**, 11243 (1989).
- [34] J. Rajeswari, P. Huang, G. F. Mancini, Y. Murooka, T. Latychevskaia, D. McGrouther, M. Cantoni, E. Baldini, J. S. White, A. Magrez, T. Giamarchi, H. M. Rønnow, and F. Carbone, *Proc. Natl. Acad. Sci. U.S.A.* **112**, 14212 (2015).
- [35] P. Milde, D. Kohler, J. Seidel, L. M. Eng, A. Bauer, A. Chacon, J. Kindervater, S. Mühlbauer, C. Pfleiderer, S. Buhbrandt, C. Schütte, and A. Rosch, *Science* **340**, 1076 (2013).
- [36] K. Tsuruta, M. Mito, H. Deguchi, J. Kishine, Y. Kousaka, J. Akimitsu, and K. Inoue, *Phys. Rev. B* **93**, 104402 (2016); K. Tsuruta, M. Mito, Y. Kousaka, J. Akimitsu, J. Kishine, and K. Inoue, Nonlinear magnetic responses in skyrmion phase of MnSi and chiral-soliton-lattice phase of Cr_{1/3}NbS₂, poster presentation at χ -Mag2016, Hiroshima, Japan (unpublished).
- [37] A. Bauer, M. Garst, and C. Pfleiderer, *Phys. Rev. Lett.* **110**, 177207 (2013).